Article

Hybrid Nanowire–Rectangular Plasmonic Waveguide for Subwavelength Confinement at 1550 Nm

Yindi Wang [ID], Hongxia Liu *[ID], Shulong Wang *[ID] and Ming Cai [ID]

Key Laboratory for Wide Band Gap Semiconductor Materials and Devices of Education Ministry,
School of Microelectronics, Xidian University, Xi'an 710071, China; wangyindi4213@126.com (Y.W.);
cm9999787@163.com (M.C.)
* Correspondence: hxliu@mail.xidian.edu.cn (H.L.); slwang@xidian.edu.cn (S.W.)

Abstract: This paper presents a hybrid waveguide based on metal surface plasmon polaritons (SPPs) at 1550 nm comprising two silver (Ag) nanowires and a rectangular silicon (Si) waveguide. Due to the strong coupling effect observed in both the metal SPP mode and Si waveguide mode, excellent waveguide characteristics, such as a small effective modal area and long transmission length, could be achieved. The research results revealed that the proposed hybrid waveguide could achieve an ultra-long transmission distance of 270 μm and normalized effective mode area of 0.01. Furthermore, the cross-sectional size of the waveguide was 500 nm × 500 nm, which helped in achieving a subwavelength size. In addition, the hybrid waveguide was resistant to manufacturing errors. These excellent performances indicate that the proposed waveguide has great application potential in optoelectronic integrated circuits.

Keywords: waveguide; SPPs; subwavelength

1. Introduction

With the recent advances in the field of optical communications, there has been an increase in the performance requirements of waveguides [1–5]. In particular, there have been rapid advances in optoelectronic integrated systems. These systems require smaller optical devices [6] to improve the system integration. Therefore, the waveguides require both a long transmission distance and small normalized mode area [7–9]. In this context, surface plasmon polaritons (SPPs) can be introduced into the waveguide design, which will help in improving the normalized effective mode area of the waveguide [10–12], thereby reducing the size of waveguide-based optical devices.

SPPs are caused by the resonance excitation of incident photons with free electron gas on a metal surface [13–16]. They are widely used for optical manipulation at the subwavelength scale because they can restrict light to a considerably smaller range than the diffraction limit [17,18]. Currently, the most widely used precious metal SPPs are gold (Au) and silver (Ag) [19]. In recent years, several types of waveguides have been designed based on SPPs [20–22], and the normalized effective mode area of waveguides has been significantly improved [10,24,25]. However, further research is required to simultaneously ensure a long transmission distance and small normalized effective mode area.

In this study, we developed a long-range hybrid waveguide operating at 1550 nm. The hybrid waveguide is composed of two Ag nanowires and a silicon (Si) waveguide. The waveguide structure has two coupling regions, which strengthens the mode coupling. Due to the strong coupling between the Ag SPPs and Si medium, the hybrid waveguide exhibits both a compact mode area and an extremely long transmission distance. The cross-sectional area of the waveguide is 500 nm × 500 nm, and a subwavelength structure is realized. Moreover, the proposed hybrid waveguide is resistant to manufacturing errors and has a wide range of applications in optical communication systems owing to its advantages.

2. Structure Design

The hybrid waveguide consists of two Ag nanowires and a conventional Si waveguide structure. The entire structure is filled with SiO$_2$ cladding, which acts as a low exponential gap between Si and Ag [23]. Excellent waveguide characteristics were obtained as a result of the double-mode coupling of Ag and Si in this structure.

The 3D structure and cross-section of the proposed hybrid waveguide are shown in Figure 1a,b, respectively. The cross-sectional area of the waveguide was 500 nm × 500 nm. Note that r_{Ag}, T_{Si}, and g denote the radius of the Ag nanowire, thickness of the rectangular Si waveguide, and gap height between the Ag nanowire and Si waveguide, respectively.
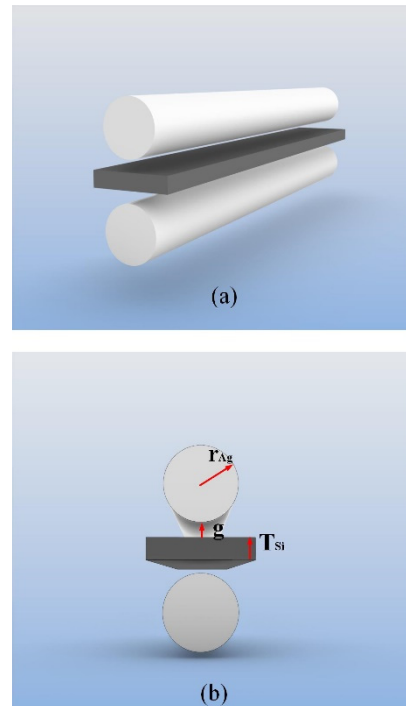

Figure 1. Structure of the proposed waveguide: (**a**) 3D layout and (**b**) cross-section.

3. Methods

The proposed hybrid waveguide utilizes the strong coupling of the Si waveguide and SPP modes to achieve good waveguide performance. It supports an ultra-long transmission distance and has an ultra-compact effective mode area. More importantly, there are two couplings in the hybrid waveguide structure. The superposition of these two couplings resulted in stronger light field localization, which helped improve the waveguide characteristics.

The properties of the hybrid waveguide can be characterized by the following four parameters: A_{eff}, L_m, *FOM*, and n_{eff} [19,24].

Here, A_{eff} is the effective modal area; its value determines the optical field constraint capability of the waveguide [25]. A smaller value of A_{eff} indicates that the light is more localized in the waveguide [26]. A_{eff} is the ratio of the total electromagnetic energy to the maximum energy density [18]. It is calculated as follows:

$$A_{eff} = \iint W(r) dA / \max(W(r)) \tag{1}$$

$$W(r) = \frac{1}{2} \mathrm{Re}\left\{ \frac{d[\omega \varepsilon(r)]}{d\omega} \right\} |E(r)|^2 + \frac{1}{2} \mu_0 |H(r)|^2 \tag{2}$$

where *H(r)* and *E(r)* represent the magnetic and electric fields, respectively. In this study, the normalized effective mode area was used; it is calculated using the formula A_{eff}/A_0, where $A_0 = \lambda^2/4$ [27].

Note that L_m represents the transmission length of the hybrid waveguide, and it is defined as follows [28]:

$$L_m = \frac{1}{2}\alpha = \lambda/4\pi\text{Im}\left(N_{eff}\right) \tag{3}$$

where N_{eff} denotes the effective modal index of the waveguide. Note that A_{eff} and L_m represent two mutually restrictive parameters, and a smaller effective modal area is often accompanied by a shorter transmission length. *FOM* is the quality factor of the waveguide, which is a tradeoff between A_{eff} and L_m. *FOM* is calculated using the following equation:

$$FOM = \frac{L_m}{2\sqrt{\frac{A_{eff}}{\pi}}} \tag{4}$$

where N_{eff} represents the loss of light in the waveguide, and n_{eff} represents the real part of N_{eff}, which can be defined as follows:

$$n_{eff} = Re(N_{eff}) \tag{5}$$

4. Results and Discussion

The hybrid waveguide utilizes the mode coupling of the Si photon and Ag nanowire plasma modes, thereby achieving excellent waveguide characteristics. Strong mode coupling can be obtained easily by adjusting the key structural parameters of the hybrid waveguide, including g, r_{Ag}, and T_{Si}.

COMSOL Multiphysics software was used for the numerical analysis of the parameters described in the methods section. In the following simulations, the incident wavelength was 1550 nm, and the relative dielectric constants of Ag, Si, and SiO_2 were $-129 + 3.3i$, 12.25, and 2.25 [18], respectively. In this study, the classical control variable method was adopted to obtain the relationship between the waveguide characteristics and parameters to optimize the waveguide characteristics.

First, the relationship between the waveguide characteristics and g was studied. Herein, g had a range of 1–20 nm. To ensure effective mode coupling and moderate transmission loss, r_{Ag} and T_{Si} were fixed at 30 and 20 nm, respectively.

As illustrated in Figure 2, with an increase in g, the normalized effective mode area, transmission length, and n_{eff} increased, whereas FOM decreased. The main reason for these results is that the coupling of the hybrid mode weakened with increasing g. The weakened mode coupling resulted in reduced light localization and an increase in the effective mode area. In turn, the length of the light transmission increased. The proposed hybrid waveguide had an extremely long transmission length (L_m: 180–270 μm) while maintaining a very small normalized effective mode area (A_{eff}/A_0: 0.01–0.05). *FOM* is a compromise between the effective mode area and transmission length. From its calculation formula, it can be observed that the *FOM* and transmission length exhibit the same change trend, and the proposed hybrid waveguide has a very high-quality factor (*FOM*: 1350–2000).
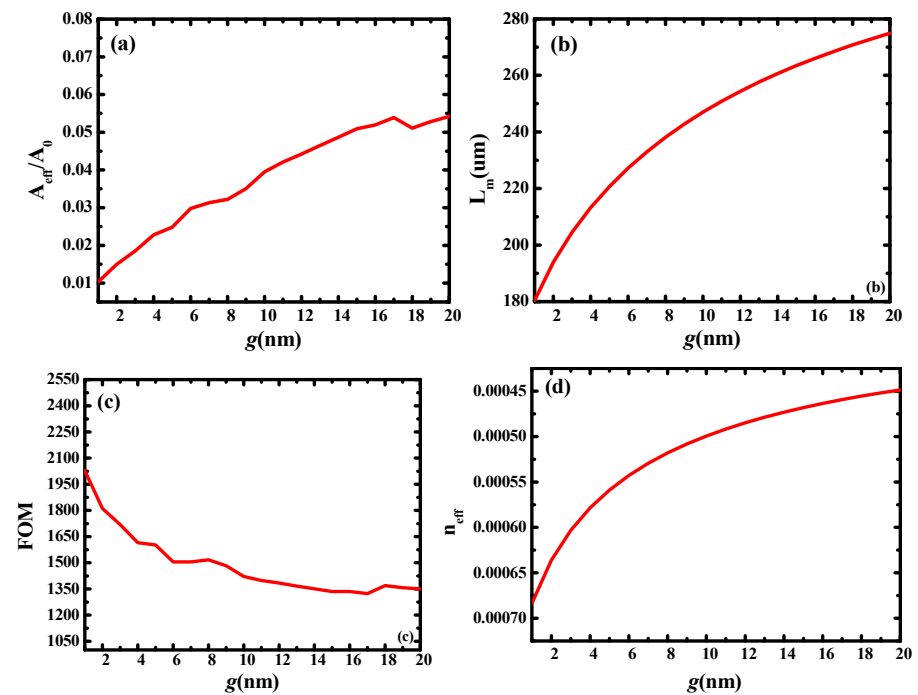
Figure 2. Dependence of waveguide characteristics on gap height (*g*): (**a**) normalized mode area (A_{eff}/A_0); (**b**) propagation length (L_m); (**c**) quality factor of waveguide (*FOM*); and (**d**) modal effective index (n_{eff}).

To further verify the abovementioned calculation results, the electric field distributions of the waveguide at different gap heights (i.e., different values of *g*) are presented. As shown in Figure 3, with an increase in *g*, the electric field distribution was increasingly diffused. The electric field was most concentrated at *g* = 5 nm, and it was concentrated in the gap region. As g increased, the electric field gradually spread beyond the gap region. This result is consistent with that shown in Figure 2. In this study, considering the characteristics of the waveguide and the actual manufacturing process, a value of 10 nm was selected for *g* in the following simulations.
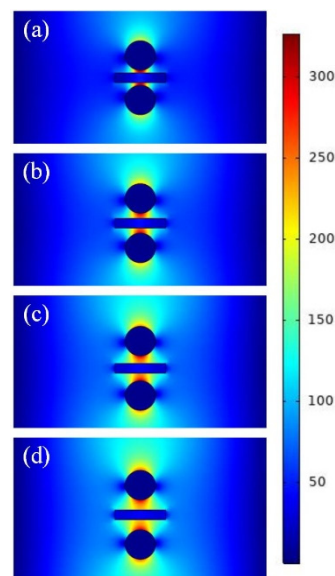

Figure 3. Electric field distributions of waveguide at different gap heights (*g*): (**a**) *g* = 5 nm; (**b**) *g* = 10 nm; (**c**) *g* = 15 nm; and (**d**) *g* = 20 nm.

Subsequently, the influence of different Si thicknesses (i.e., different values of T_{Si}) on the waveguide characteristics was investigated. In this calculation, the value of T_{Si} varied in the range of 1–30 nm, r_{Ag} was 30 nm, and g was 10 nm. The results are shown in Figure 4, wherein, it can be observed that the characteristics of the hybrid waveguide were only slightly affected by the Si thickness because it had no effect on the coupling of the two hybrid modes.
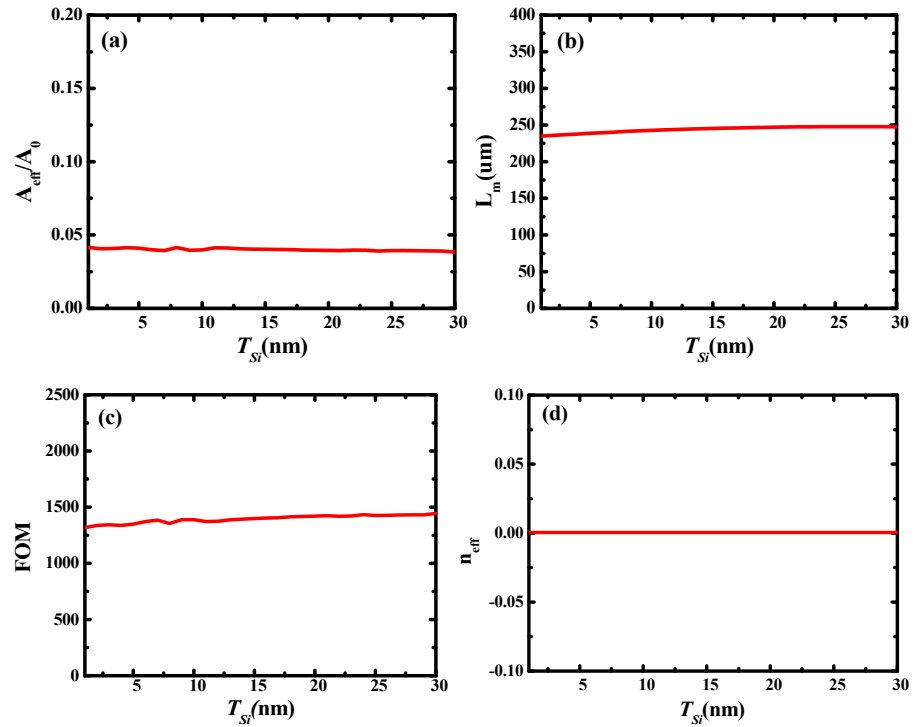

Figure 4. Dependence of waveguide characteristics on Si thickness (T_{Si}): (**a**) normalized mode area (A_{eff}/A_0); (**b**) propagation length (L_m); (**c**) quality factor of waveguide (*FOM*); and (**d**) modal effective index (n_{eff}).

To verify the above conclusions, the electric field distributions for different Si thicknesses were obtained. Here, Figure 5a–c show the electric field distributions at different values of T_{Si}. It can be observed that for different Si thicknesses, the electric field of the waveguide did not diffuse, and the light was well localized. This is consistent with the calculation results shown in Figure 4. Therefore, we fixed T_{Si} at 20 nm in the following simulations.
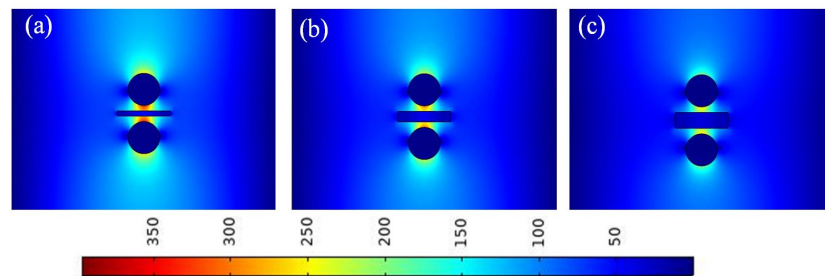

Figure 5. Electric field distributions at different Si thicknesses (T_{Si}): (**a**) T_{Si} = 10 nm; (**b**) T_{Si} = 20 nm; and (**c**) T_{Si} = 30 nm.

Subsequently, the effect of the radius of the Ag nanowires (r_{Ag}) on the waveguide characteristics was explored. Here, r_{Ag} had a range of 10–100 nm, and g and T_{Si} were fixed

at 10 and 20 nm, respectively. Figure 6a–d show the dependence of A_{eff}/A_0, L_m, *FOM*, and n_{eff} on r_{Ag}, respectively. It can be observed that the effective mode area (A_{eff}/A_0) was very large, and the transmission distance (L_m) was short in the region where r_{Ag} was less than 20 nm and r_{Ag} was greater than 75 nm. The primary reason for this phenomenon is that no mode coupling occurred in this region. Furthermore, the waveguide exhibited good characteristics when r_{Ag} was in the range of 20–75 nm. This is due to the strong mode coupling occurring in this region.
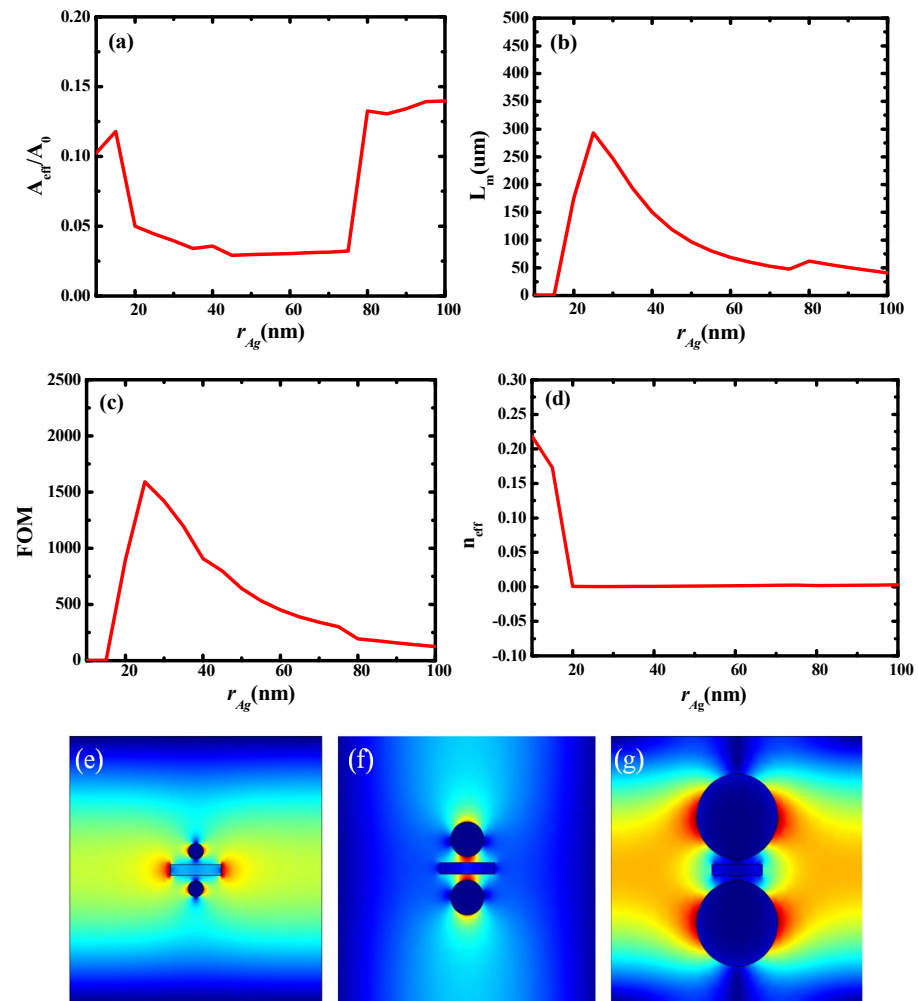

Figure 6. Dependence of waveguide characteristics on radius of Ag nanowires (r_{Ag}): (**a**) normalized mode area (A_{eff}/A_0); (**b**) propagation length (L_m); (**c**) quality factor of waveguide (*FOM*); (**d**) modal effective index (n_{eff}); (**e**) electric field distributions at r_{Ag} = 15 nm; (**f**) electric field distributions at r_{Ag} = 30 nm; and (**g**) electric field distributions at r_{Ag} = 80 nm.

Here, Figure 6e–g show the electric field distributions at r_{Ag} = 15, 30, and 80 nm, respectively. It can be observed that at r_{Ag} = 15 and 80 nm, no coupling occurred, and the electric field was dispersed in the cladding, whereas at r_{Ag} = 30 nm, mode coupling occurred, and the electric field was concentrated in the gap region. This is consistent with the calculation results shown in Figure 6a–d.

Figure 7 shows the electric field distributions at different values of r_{Ag} (20–70 nm). As r_{Ag} increased, the electric field became more localized because a larger radius of the Ag nanowires leads to stronger mode coupling. Considering this observation in combination with the results observed in Figure 6, a value of 30 nm was selected for r_{Ag} in the following simulations.
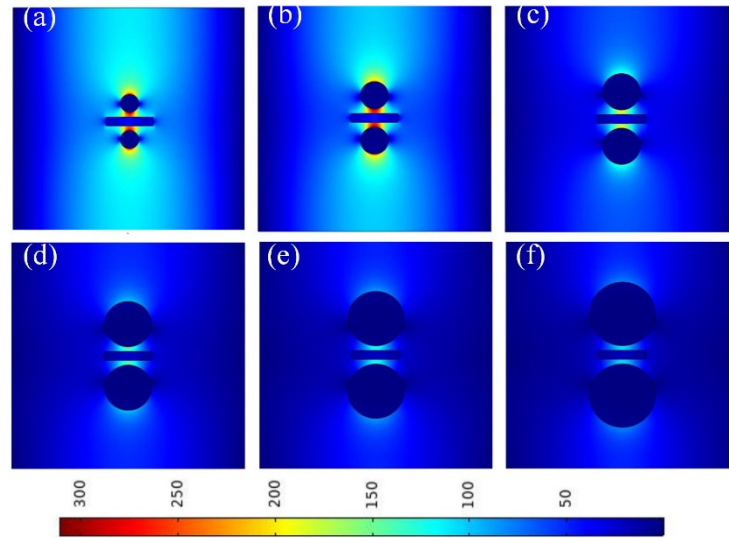
Figure 7. Electric field distributions at different values of r_{Ag}: (**a**) r_{Ag} = 20 nm; (**b**) r_{Ag} = 30 nm; (**c**) r_{Ag} = 40 nm; (**d**) r_{Ag} = 50 nm; (**e**) r_{Ag} = 60 nm; and (**f**) r_{Ag} = 70 nm.

Based on the aforementioned results, it can be concluded that the characteristics of the waveguide can be optimized by adjusting the geometric parameters. Thus, the proposed hybrid waveguide exhibited a small effective mode area and an ultra-long transmission distance.

5. Fabrication Processing and Fabrication Error Tolerance

After all the geometric parameters were determined, a hybrid waveguide was fabricated using the standard micromachining process [29,30]. All the geometric parameters of the waveguide could be precisely controlled, except for the central symmetry of the two Ag nanowires. Next, we investigated the difference in waveguide characteristics caused by the deviation of the center position of the two Ag nanowires (dx). In this simulation, g, r_{Ag}, and T_{Si} were 10, 30, and 20 nm, respectively. As shown in Figure 8, the center asymmetry error, dx (1–30 nm), caused errors of only 7% and 2.4% for A_{eff}/A_0 and L_m, respectively.

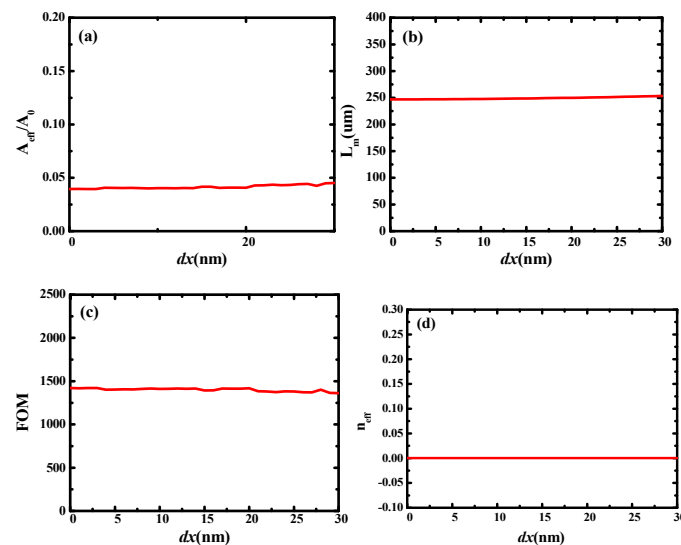**Figure 8.** Dependence of waveguide properties on central symmetric error (dx): (**a**) normalized mode area (A_{eff}/A_0); (**b**) propagation length (L_m); (**c**) quality factor of waveguide (*FOM*); and (**d**) modal effective index (n_{eff}).

Figure 9 shows the electric field distributions at different values of *dx* (10, 20, and 30 nm). As *dx* increased, the waveguide maintained strong mode coupling and good electric field localization, which is consistent with the results observed in Figure 8. These results showed that the hybrid waveguide is reliable and robust against manufacturing errors.
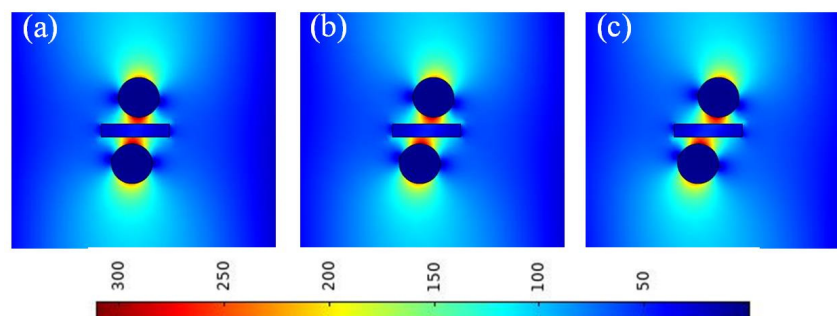

Figure 9. Electric field distributions at different values for *dx*: (**a**) *dx* = 10 nm; (**b**) *dx* = 20 nm; and (**c**) *dx* = 30 nm.

6. Conclusions

In this study, a hybrid waveguide based on metal SPPs and operating at 1550 nm was proposed. The hybrid waveguide achieved both a small effective modal area and long transmission length using the strong coupling between the metal SPP mode and Si waveguide mode. The results showed that the waveguide achieved an ultra-long transmission distance of 270 μm and effective mode area of 0.01. The cross-sectional size of the waveguide was only 500 nm × 500 nm, which realized a subwavelength size. The results showed that the properties of the proposed waveguide are resistant to manufacturing errors. These excellent performances indicate that the proposed waveguide has great application potential in optoelectronic integrated circuits.

Author Contributions: Y.W. wrote the main manuscript text and performed the simulations and calculations. H.L. and S.W. gave the constructive suggestion. Other authors edited the manuscript. All authors have read and agreed to the published version of the manuscript.

Institutional Review Board Statement: Not applicable.

Informed Consent Statement: Not applicable.

Data Availability Statement: Not applicable.

Conflicts of Interest: The authors declare no conflict of interest.

References

1. Ferreira, P.; Almeida, G.; Mendona, C.R. A simple strategy for increasing optical waveguide performance using spherical aberration. *Opt. Laser Technol.* **2021**, *142*, 107235. [CrossRef]
2. Chandra, V.; Ranjan, R. Performance analysis of different slot waveguide structures for evanescent field based gas sensor applications. *Opt. Quantum Electron.* **2021**, *53*, 1–5. [CrossRef]
3. Arianfard, H.; Wu, J.; Juodkazis, S.; Moss, D.J. High Performance Optical Filters Using Three Waveguide Coupled Sagnac Loop Reflectors. *arXiv* **2021**, arXiv:2103.07822.
4. Oulton, R.F.; Sorger, V.J.; Genov, D.A.; Pile, D.F.P.; Zhang, X. A hybrid plasmonic waveguide for subwavelength confinement and long-range propagation. *Nat. Photonics* **2008**, *2*, 496–500. [CrossRef]
5. Dai, D.; He, S. A silicon-based hybrid plasmonic waveguide with a metal cap for a nano-scale light confinement. *Opt. Express* **2009**, *17*, 16646–16653. [CrossRef] [PubMed]

6. Chan, S.J. Automated inspection systems for the electronics industry: As IC devices get smaller and smaller, the challenge of detecting faults becomes bigger and bigger. *EE-Eval. Eng.* **2005**, *44*, 56–59.

7. Hu, Y.-J.; Xu, L.; Zhang, Q.; Yuan, C.-W.; Liu, J.-L.; Sun, Y.-F. A compact high-power microwave TM01-TE01 mode converter. *Rev. Sci. Inst.* **2021**, *92*, 094703. [CrossRef] [PubMed]

8. Rui, X.; Jian, S. The Graphene Square Waveguide with Small Normalized Mode Area. *IEEE Photonics Technol. Lett.* **2017**, *29*, 1643–1646.

9. Singh, R.; Priye, V. Si_3N_4—SiO_2 Based Curve Slot Waveguide for High Confinement Factor and Low Mode Effective Area along with Biosensing Application. *Silicon* **2021**, *14*, 859–867. [CrossRef]

10. He, X.; Liu, F.; Lin, F.; Shi, W. Tunable 3D Dirac-semimetals supported mid-IR hybrid plasmonic waveguides. *Opt. Lett.* **2021**, *46*, 472–475. [CrossRef]

11. Teng, D.; Wang, K.; Huan, Q.; Chen, W.; Li, Z. High-performance light transmission based on graphene plasmonic waveguides. *J. Mater. Chem. C* **2020**, *8*, 6832–6838. [CrossRef]

12. Teng, D.; Wang, K. Theoretical Analysis of Terahertz Dielectric–Loaded Graphene Waveguide. *Nanomaterials* **2021**, *11*, 210. [CrossRef] [PubMed]

13. Cuevas, M.; Depine, R.A. Excitation of surface plasmon polaritons along the sinusoidal boundary of a metamaterial. *Phys. Rev. B Condens. Matter* **2008**, *78*, 125412. [CrossRef]

14. Tgab, C.; Erb, D. Propagation of surface plasmon polaritons at the interface of metal-free metamaterial with anisotropic semiconductor inclusions. *Optik* **2022**, *254*, 168678.

15. Wang, Y.; Liu, H.; Wang, S.; Cai, M.; Ma, L. Optical Transport Properties of Graphene Surface Plasmon Polaritons in Mid-Infrared Band. *Crystals* **2019**, *9*, 354. [CrossRef]

16. Teng, D.; Wang, Z.; Huan, Q.; Wang, H.; Wang, K. A low loss platform for subwavelength terahertz graphene plasmon propagation. *Opt. Mater.* **2022**, *128*, 112436. [CrossRef]

17. Wang, Y.; Wang, S.; Cai, M.; Liu, H. A Long Propagation Distance Hybrid Triangular Prism Waveguide for Ultradeep Subwavelength Confinement. *IEEE Sens. J.* **2019**, *19*, 11159–11166. [CrossRef]

18. Lu, D.; Liu, H.; Wang, S.; Sheng, Q.; Lei, W. Hybrid Tube-Triangle Plasmonic Waveguide for Ultradeep Subwavelength Confinement. *J. Lightwave Technol.* **2017**, *35*, 2259–2265.

19. Bian, Y.; Ren, Q.; Kang, L.; Yue, T.; Werner, P.L.; Werner, D.H. Deep-subwavelength light transmission in hybrid nanowire-loaded silicon nano-rib waveguides. *Photonics Res.* **2018**, *6*, 37–45. [CrossRef]

20. Zhou, T.; Gou, X.; Xu, W.; Li, Y.; Zhai, X.; Li, H.; Wang, L. Dynamically Tunable Plasmon-induced Transparency in a T-shaped Cavity Waveguide Based on Bulk Dirac Semimetals. *Plasmonics* **2021**, *16*, 323–332. [CrossRef]

21. Qiao, Q.; Xu, Y.; Zhang, L.; Li, W.; Shi, Z. Spoof surface plasmon polariton waveguide with spiral structure units. *Eur. Phys. J. Plus* **2021**, *136*, 874. [CrossRef]

22. Teng, D.; Wang, K.; Li, Z. Graphene-Coated Nanowire Waveguides and Their Applications. *Nanomaterials* **2020**, *10*, 229. [CrossRef] [PubMed]

23. Huang, J. Terahertz graphene modulator based on hybrid plasmonic waveguide. *Phys. Scr.* **2021**, *96*, 125525. [CrossRef]

24. Ma, Y.; Farrell, G.; Semenova, Y.; Wu, Q. Hybrid nanowedge plasmonic waveguide for low loss propagation with ultra-deep-subwavelength mode confinement. *Opt. Lett.* **2014**, *39*, 973–976. [CrossRef]

25. Dan, X.; Huang, Y.; Wang, X.; Hao, H.; He, H. Hybrid Surface Plasmon Polariton Waveguide of Low-Loss and Ultra-Small Modal Area. *Acta Opt. Sin.* **2015**, *35*, 0623003. [CrossRef]

26. Ma, Z.A.; Zhang, P.B.; Li, L.; Ni, X.A. Endless single-polarization single-mode photonic-crystal planar waveguide arrays with ultra-large mode area and ultra-low transmission loss—ScienceDirect. *Optik* **2021**, *238*, 166474. [CrossRef]

27. Kumar, S.; Kumar, P.; Ranjan, R. A Metal-Cap Wedge Shape Hybrid Plasmonic Waveguide for Nano-Scale Light Confinement and Long Propagation Range. *Plasmonics* **2021**, *17*, 95–105. [CrossRef]

28. Wang, Y.; Liu, H.; Wang, S.; Cai, M. A waveguide-integrated graphene-based subwavelength electro-optic switch at 1550 nm. *Opt. Commun.* **2021**, *495*, 127121. [CrossRef]

29. Tilmans, H.; Baert, K.; Verbist, A.; Puers, R. CMOS foundry-based micromachining. *J. Micromech. Microeng.* **1996**, *6*, 122. [CrossRef]

30. Mohammad, T.; He, S.; Mrad, R.B. Conventional surface micromachining process for the fabrication of a linear optical phased array based on piston micromirrors. *J. Micromech. Microeng.* **2021**, *31*, 065009. [CrossRef]